SLAC-PUB--5365-Rev.

DE91 009365

Component and System Tests of the SLD Cerenkov Ring Imaging Detector*

P. Antilogus,[a] D. Aston, T. Bienz,[b] F. Bird[a] S. Dasu, S. Dolinsky,[c] W. Dunwoodie, G. Hallewell, H. Kawahara, Y. Kwon, D. Leith, D. Muller,[**] T. Nagamine, T. Pavel, B. Ratcliff, P. Rensing, D. Schultz, S. Shapiro, C. Simopoulos, E. Solodov,[d] N. Toge, J. Va'vra, and S. Williams
Stanford Linear Accelerator Center, Stanford University, Stanford, CA 94309, USA

M. Cavalli-Sforza, P. Coyle,[e] D. Coyne, P. Gagnon, X. Liu, and D. A. Williams
Santa Cruz Institute for Particle Physics, University of California, Santa Cruz, CA 95064 USA

J. S. Whitaker and R. J. Wilson
Department of Physics, Boston University, Boston, MA 02215, USA

A. Bean, D. Caldwell, J. Duboscq, J. Huber, A. Lu, L. Mathys, S. McHugh, M. Witherell, and S. Yellin
Department of Physics, University of California, Santa Barbara, CA 93106, USA

A. d' Oliveira, R. A. Johnson, J. L. Martinez, B. Meadows, M. Nussbaum, A.K.S. Santha, A. Shoup, and I. Stockdale
Department of Physics, University of Cincinnati, Cincinnati, OH 45221, USA

K. Baird, P. Jacques, M. Kalelkar, R. Plano, P. Stamer, and G. Word
Serin Physics Laboratory, Rutgers University, P.O. Box 849, Piscataway, NJ 08855, USA

K. Abe, K. Hasegawa, F. Suekane, and H. Yuta
Department of Physics, Tohoku University, Aramaki, Sendai 980, JAPAN

Abstract

The components of the SLD barrel Cerenkov Ring Imaging Detector (CRID) are now built and are being installed. We report on tests of these, including tests of the fiber optic calibration system, detailed studies of electron drift paths on production drift boxes and detectors, tests of the dynamic gating system and its effect on drift path distortions due to space-charge, and a measurement of the electron lifetime in a production drift box. In addition, we report on the UV transmission of recirculated liquid C_6F_{14} and on the effects of CRID construction materials on electron lifetime.

I. Introduction

The components of the SLD barrel CRID [1,2] are now completed and are in the process of installation in the SLD detector. The barrel CRID (Fig. 1) will provide SLD with excellent particle identification over the central 70% of the solid angle. The combination of gaseous and liquid radiators will allow $\pi/K/p$ separation up to more than 30 GeV/c and e/π separation up to about 6 GeV/c.

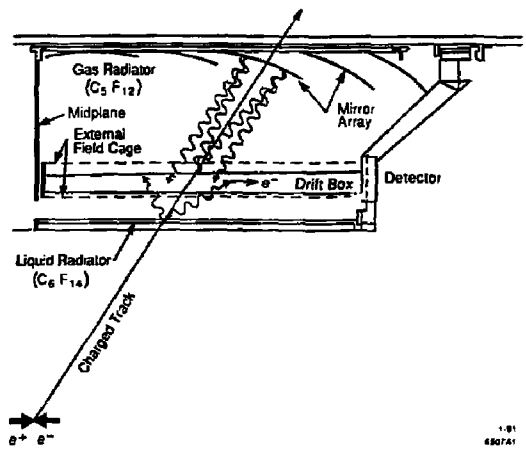

Fig. 1 Quarter section of the SLD Barrel CRID showing its principal components. There are ten azimuthal sectors on each side of the midplane.

Figure 1 shows a section of the barrel CRID, which consists of a large vessel that will be filled with the gaseous radiator C_5F_{12} and held at 40°C, well above the C_5F_{12} boiling point of 30°C. Inside are ten azimuthal sectors on each side of the midplane, each consisting of two liquid radiator trays, two drift boxes, and four rows of five mirrors. The liquid radiators are a 1-cm-thick layer of C_6F_{14} contained in a 124 by 34 cm tray. The side of the tray facing away from the beam is quartz, which is transparent to the expected Cerenkov photons. The other

*Work supported in part by Department of Energy contracts DE-AC03-76SF00515 (SLAC) and DE-AT03-79ER70023, and by National Science Foundation grants PHY88-13669 and PHY88-13018.

[a] Present Address: EP Division, CERN, CH-1211, Geneva 23, Switzerland.

[b] Present Address: University of Iowa, Iowa City, IA, USA.

[c] Permanent Address: Inst. of Nuclear Physics, Novosibirsk, 630090, USSR.

[**] Speaker.

[e] Present Address: Centre de Physique des Particules, Faculte des Sciences de Luminy, IN^2P^3-CNRS, 13288, Marseille, France.

Presented at the 1990 IEEE Nuclear Science Symposium, Arlington, VA, October 23–26, 1990.

sides are G-10 fiberglass-epoxy.[1] Photons produced in the liquid are proximity focused onto the near side of the drift box, and those produced in the gas are focused by the spherical mirrors onto the far side.

The drift box is a 127-cm-long by 30-cm-wide time projection chamber containing ethane with about a 0.1% admixture of tetrakis[dimethylamino]ethylene (TMAE), which can be ionized by Cerenkov photons with wavelength below 230 nm to yield single electrons. The inner and outer sides are quartz, the other sides G-10. The photoelectrons drift away from the midplane, toward a single electron detector [3], a multiwire proportional chamber with 7 μm carbon fiber anodes with 3.2 mm pitch. The readout electronics are described in ref. [4]. The depth of the drift box is tapered, increasing from 6 cm at the midplane to 10 cm at the detector, to ensure that drifting electrons do not diffuse onto the quartz windows.

The three production coordinates of each photoelectron are determined to an accuracy of 1 mm from the drift time, the anode fiber address, and by charge division along the fiber. Reconstructed Cerenkov photons are matched to charged tracks found in the SLD Central Drift Chamber (CDC) [1] and their Cerenkov angles are calculated. These angles measure the particle velocity, which, together with the momentum measurement in the CDC, determines the particle mass.

The components undergo rigorous testing, much of which has been reported previously [3,5]. We present here several new results concerning drift boxes: first tests of the fiber optic calibration and drift velocity monitoring system on a drift box; first tests of the dynamic gating system on a drift box—in particular, its ability to prevent drift path distortions due to space-charge; first detailed maps of drift paths in production drift boxes; and measurements of the electron attachment lifetime in a drift box. In addition, we present tests of the effects of materials used in CRID construction on UV transparency of the liquid radiator C_6F_{14} and on the electron lifetime, and tests of the liquid recirculation system.

II. The Drift Box Test Setup

Extensive tests of drift box and detector systems have been made with the apparatus shown in Fig. 2. A drift box and detector are held at 40°C surrounded by Freon 114 for high voltage safety in a Lucite box. Prototype data acquisition and gas monitoring systems are connected. A UV flashlamp (not shown) and 600 μm optical fiber are used to input light to the fiber optic calibration system, as described in the next section. Alternatively, the box can be illuminated by a nitrogen laser ($\lambda = 337$ nm), which is movable across the top of the box (the x-y plane) and free to rotate in the y-z plane. By comparing reconstructed lines with those of known position from the optical fibers or laser, the drift field can be mapped. Since it is not practical to map the field in all the production drift boxes, one aim of our tests is to verify that the optical fiber system provides an adequate field map. Also, a few boxes are being mapped more extensively with the movable laser in order to better understand the information from the limited number of fibers.

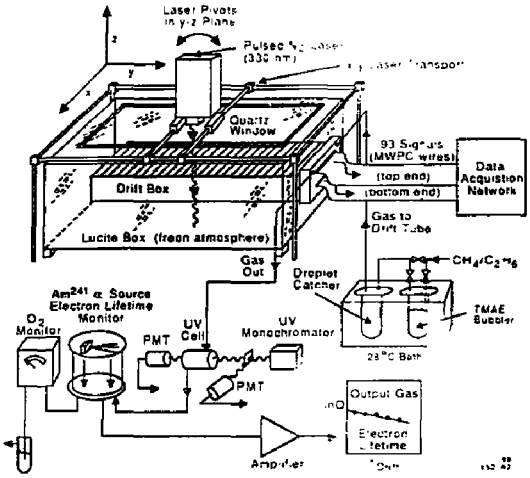

Fig. 2 The test apparatus for drift boxes and the prototype gas monitoring system.

III. The Fiber Optic Calibration System

A system of optical fibers will provide fiducial lines in the drift boxes. Figure 3 shows a schematic of this system: a UV flashlamp[2] illuminates a set of 600-μm core-diameter Fiberguide UV-transmitting optical fibers,[3] one for each drift box. Each of these fibers illuminates a bundle of nineteen 200 μm fibers,[4] which penetrates the main vessel volume at the outer edge of the drift box. The other ends of these fibers are held by collimators glued at several points on the quartz window facing the mirrors. The black Delrin plastic collimators have a 0.012-inch-diameter hole at the quartz window that produces a beam with angular divergence 34 to 44 mrad. The error in centering the fiber leads to an uncertainty of about 15 mrad in the angle of the beam.

The arrangement of fibers on each drift box is shown in the lower part of fig. 3. There are three different orientations: eight beams are directed perpendicular to the quartz window (indicated by dots in the figure) and are used continuously to monitor the electron drift velocity.

1 NVF Technical Products, Kennet Square, PA

2 Hamamatsu model L2435

3 Model SFS600Z, Fiberguide Industries, Stirling, NJ

4 Model SFS200Z, Fiberguide Industries, Stirling, NJ

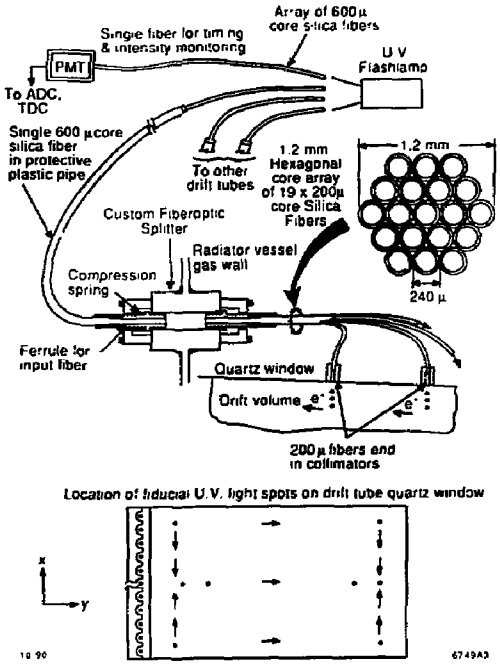

Fig. 3 The fiber optic calibration system.

which must be known to 0.1% to achieve 1 mm production point accuracy at the longest drift. The remaining fibers are angled at 45° with respect to the quartz window, in the planes indicated by the arrows in fig. 3. The four fibers nearest the detector and angled perpendicular to it are used to check the charge division calibration of the wires, which must be known to 1%. The remaining angled fibers are used to measure drift path distortions in the depth coordinate, z, and all fibers are used to measure distortions in the width coordinate, x.

The throughput of UV light in this system is very sensitive to the surface quality of the ends of the fibers, as well as to their alignment with the flashlamp and with each other in the bulkhead. With careful polishing of all ends, enough light is provided by the Hamamatsu flashlamp to see more than one hit in the drift box per fiber per flash, more than sufficient for our purposes. A more difficult problem is to make the light output of each fiber in a given bundle of 19 uniform. The transmission of short segments such as used here is subject to large variations from the manufacturing process. The uniformity also depends on end-surface quality, alignment, and a limiting radius of curvature of the 200 μm fibers. In bench tests of finished bundles, the brightest fiber is two to six times more transmissive than the dimmest, and the standard deviation of the light outputs is typically 50% of the mean.

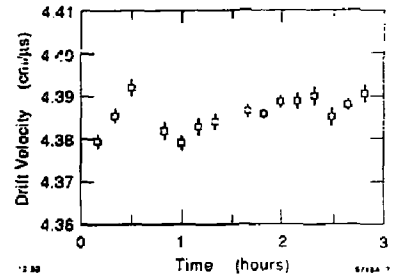

Fig. 4 Drift velocity measured with the fiber optic system over a three-hour period.

The uniformity of light output from box to box will be obtained by adjusting the distance of each 600-μm-fiber from the flashlamp.

Initial tests of the fiber optic system indicate that it will satisfactorily perform its primary role of accurately monitoring drift velocities with sets of about 1000 shots taken hourly. Figure 4 shows results of a test using sets of 1000 shots taken in ten minute runs. The average arrival time of signals from each of the four vertical fibers along the central drift axis is found, and a line fitted to find the drift velocity. Statistical accuracy below the 0.1% requirement is seen. The gradual increase is consistent with temperature and pressure variation in the test setup.

The charge division calibration and drift paths are checked in dedicated runs during down time. Tests of the calibration check have shown that the 1% requirement can be achieved on all wires in several minutes of running.

Drift path measurements have been made with the fibers on two boxes and agree with laser data. Figure 5 is an example of such a measurement, using the central angled fiber. The reconstructed hits are binned by arrival time, and the average depth, z, is found for each bin. The rate is kept low (about 0.1 hits per flash), to keep to a minimum multiple hits which might overlap. The average depths are expected to fall on a line of known slope, given by the fiber angle and measured drift velocity. The dashed line in fig. 5(a) has this slope, and its intercept has been fitted to the central region of the data. Figure 5(b) shows the residuals, or z-distortion, in millimeters. The horizontal axis has been converted to the expected z value. The z-distortion is typically below 1 mm which is acceptable. This is achieved by careful matching of the electric fields in the drift region and the detector [2,5]. This adjustment is available to each drift box in the barrel CRID, and will be made based on optical fiber data.

IV. Gating Circuit Tests

The detector is gated to prevent positive ions produced in avalanches from entering the drift volume and affecting electron drift paths. A section of the detector

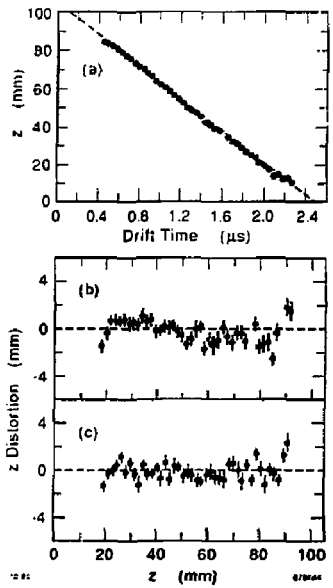

Fig. 5 A z-distortion measurement from the central optical fiber: (a) average depth versus arrival time; (b) residuals versus expected depth; (c) same as (b), but ungated.

is shown in Fig. 6., together with simulated drift trajectories for the two electrostatic configurations of the gate. The cathode is at the bottom of the figure. The lower row of dots represents the anode carbon fibers. The series of rectangular pieces are blinds which reduce photon feedback. The top row of dots are the gate wires. In the open configuration, the gate wires are held at a constant voltage of −4.2 kV, and both electrons and positive ions are free to drift through. When the gate closes, an additional bias of ±350 V is applied to alternate wires, preventing the drift of charged particles through the gate.

The SLC will provide beam crossings at a rate of 120 Hz. The gate is held open for 50 μs after each crossing to admit electrons drifting the full length of the box. Since the positive ions drift much more slowly than electrons, the gate will be closed by the time they reach it and none will enter the drift volume. In addition, most of the non-beam-related background ionization will be gated away, increasing the lifetime of the detectors.

Tests of the gating in static mode have been reported [6]. The final gating circuit prototype is used in the above setup, the gate opening 120 times per second for about 150 μs, with laser or optical fiber shots coming 75 μs before closing. If the gating circuit is turned off (gate always open), then fig. 5(b) becomes fig. 5(c). There is a very small difference between the two, which may be attributed to the space-charge due to cosmic rays.

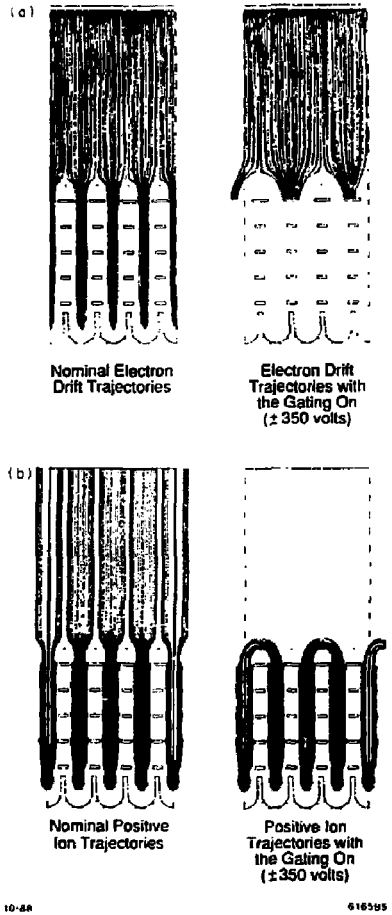

Fig. 6 Geometry of the single electron detector, including simulated drift trajectories for (a) electrons and (b) positive ions with gates open and closed.

In a more severe test of the gating circuit, a continuous UV lamp is used to flood the drift volume with space-charge: the aperture of the lamp is adjusted to illuminate the region close to the detector in y uniformly in x-z. Photoelectrons are copiously produced and, with the gating off, drift in and avalanche, producing positive ions which fill the drift volume more or less uniformly. The intensity of the lamp is varied and the space-charge density monitored by measuring the current drawn by the cathode, using a custom nanoammeter [7]. Figure 7 shows the z-distortion measured in the center of the drift box for several different space-charge densities. The solid lines are the result of a simulation. The density normalization is derived from the simulation, and agrees to within 20% with a rough

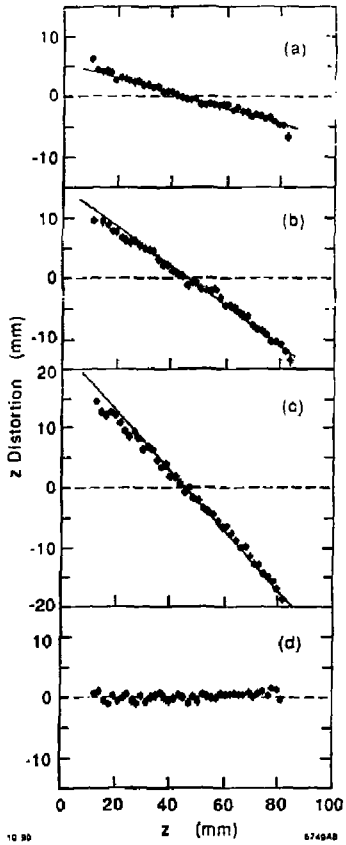

Fig. 7 z-distortion measured with space-charge densities of (a) 0.5, (b) 1.5, (c) 2.5×10^6 ions per cm^3 (the solid lines are results of an electrostatic simulation), and (d) measured under the same conditions as (c) except that the gating has been turned on.

calculation based on the cathode current. Large distortions are observed which increase with charge density. When the gating is turned on, the cathode current drops to the expected 2% of its previous value and these distortions disappear [Fig. 7(d)]. Similar effects were observed for distortions in the x-direction. The drop in cathode current indicates that the gate effectively prevents electrons from entering while closed. They do enter during the 2% open time and avalanche, but the gate closes before the positive ions can return to the drift volume, as evidenced by the complete elimination of distortions.

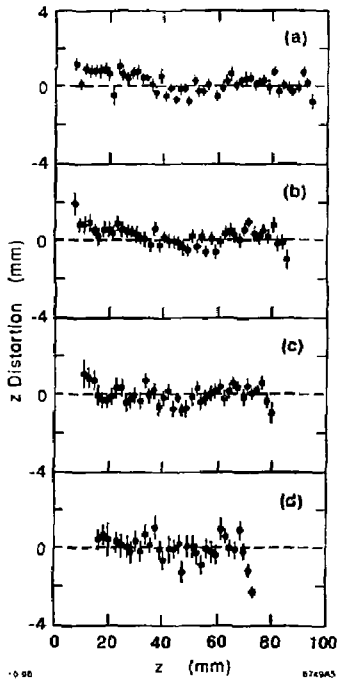

Fig. 8 z-distortion measurements along the box centerline for drift distances of (a) 7, (b) 42, (c) 78, and (d) 117 cm.

V. Mapping the Drift Field

To meet the physics goals of the CRID detector, the path of an electron's drift in the drift boxes, nominally parallel to the beam, must be known to 1 mm in the transverse directions. We have seen [5] that distortions are small throughout the main volume of the drift boxes tested. Two production boxes have been mapped in more detail near all the sides. We present measurements on the worse of the two boxes tested.

The drift path maps were made with the laser at a 45° angle in the y-z plane, and at various positions in x-y. Measurements were first made in the center of the drift box and found to agree with optical fiber data. Figure 8 shows that no visible distortion develops with longer or shorter drift distance along the central line. The domain of the data varies because of the taper in the box depth. No change is observed until the sidewalls in x are approached. Figure 9 shows some structure developing with drift distance at 1.2 cm (3.5 wires) from one side. These distortions increase rapidly as the side is approached.

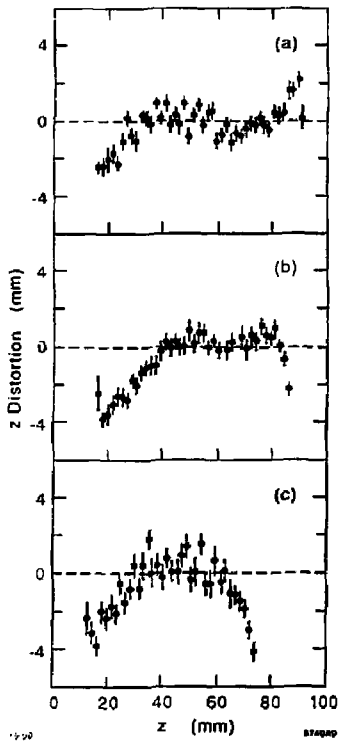

Fig. 9 z-distortion measurements 1.2 cm from one side of a drift box for drift distances of (a) 42, (b) 78, and (c) 117 cm.

Distortions up to 6 mm have been observed at this side. Typically, the maximum on a side is 2 to 3 mm.

The photoelectrons from a given laser line typically reach 2 to 4 wires due to finite beam radius and diffusion. The average arrival position in the x-direction of many signals can therefore be found to better than the wire pitch, and drift distortions in this direction measured. Along the centerline, the drift may be at a slight angle in x-y, due to misalignment of the field-shaping arrays. This is measured with the central optical fibers to be less than 1 mrad in the two boxes tested, and so other measurements are referenced to the centerline. Distortions in x are then found to be small in most of the box volume, with the exception of the region near the side walls. Figure 10 shows the difference between measured and expected average x position as a function of distance from one side wall, for drift over (a) one-half and (b) the full length of the box. A positive distortion here is toward the center of the box. Distortions depend on depth, are small except on a few wires near the edge, and reach a maximum of 2 to 3 mm

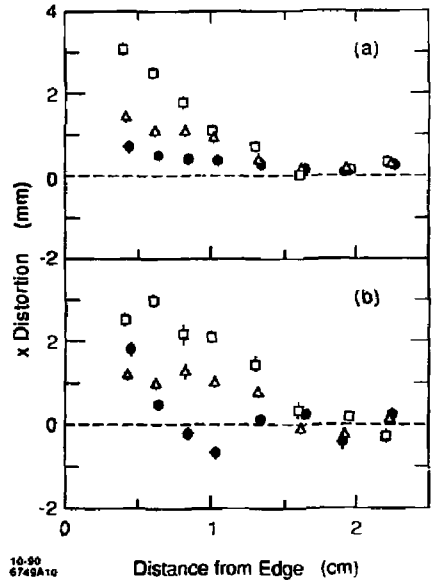

Fig. 10 x-distortion measurements as a function of expected x-position near the bottom (squares), middle (triangles) and top (solid circles) of a drift box, and for (a) 60 and (b) 117 cm drift.

on the boxes studied so far. Overall, distortions in both transverse directions are small, reasonably well-behaved, and appear to be correctable at the millimeter level almost everywhere in these two boxes.

VI. Measurement of the Electron Lifetime

The small number of Cerenkov photoelectrons produced requires that photoelectrons reach the detector efficiently. We are therefore very sensitive to the presence of impurities in the gas and to the electron capture properties of the drift gases, ethane and TMAE. In particular, fluorocarbons capture electrons very well [8], and the Freon atmosphere in the test setup serves as a very stringent leak test. Both the test setup and CRID are equipped with electron lifetime monitors (see next section), which are useful for spotting changes in the lifetime in the output gas. However, it is desirable to measure this quantity directly in a production drift box.

The efficiency with which photoelectrons reach the detector can be measured as a function of drift distance, using either the laser or optical fibers as input. The systematic accuracy with which the number of photoelectrons produced at each point can be known is limited to a few percent by the unstable intensity of the flashlamp and

laser, the nonuniform transparency of the quartz windows, and uncertainty in the correction for the varying depth of the drift box. Therefore, we cannot reliably measure lifetimes long compared to the time required to drift the full length of the box.

Different gases can be compared using the optical fibers. The relative illumination of each is not measurable to the required accuracy, but should not change over the long time needed for statistics and gas changeover, if the input optics remain constant. Since the fibers are illuminated simultaneously, the comparison is insensitive to fluctuations in the lamp intensity. We have compared the ratio of signal rates from the central fibers at each end of the drift box for pure ethane and for ethane plus 0.1% TMAE, and found a $5 \pm 4\%$ decrease with the addition of TMAE over a drift time of 25 μs. The error has about equal statistical and systematic contributions. Thus, the TMAE and any impurities it introduces capture electrons at a slow rate, less than about 0.004 per μs.

It is possible to observe a lifetime by increasing the total drift time, *i.e.*, by reducing the drift field. At these relatively low fields, the lifetime is not expected to depend on the drift field. We have made measurements of the lifetime using the laser at several drift field values, which are shown in Fig. 11. Only statistical errors are shown. We estimate systematic errors on each point, as well as an overall systematic error of about 50 μs. There are three measurements at the full drift field, one of which gives almost infinite lifetime, and one of which (the open circle) was made without TMAE in the gas. The three cover a wide range, but are indistinguishable within errors. However, the other measurements are reasonable, and the lifetime does not appear to depend on the drift field over this range. In no case is the measured lifetime below 200 μs. A weighted average of the lifetimes in the plot yields $300 \pm 20 \pm 60$ μs, where the first error is statistical and the second is a coarsely estimated systematic. This lifetime corresponds to ten times the drift time for the length of a drift box, which is more than adequate for the CRID.

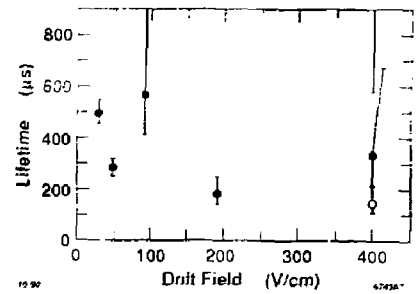

Fig. 11 Electron lifetime measured for various drift fields. The open circle is a measurement for pure ethane, the rest for ethane plus 0.1% TMAE.

VII. Drift Box and Detector Materials Tests

Building instruments that will be exposed to TMAE vapors requires careful choice of materials and cleaning procedures, because TMAE is a rather unstable chemical; it reacts with oxygen in the presence of a few parts per million of water or alcohol, and reacts with common plastics and composite materials. Some TMAE reaction products have high electron affinity, leading to intolerable losses of Cerenkov photoelectrons, by attachment to molecules of TMAE decomposition products during drift to the electron detector [9]. For this reason, we have tested every component used in drift box or detector construction for adverse effects on electron drift lifetimes.

The method is based on an ionization chamber, the electron lifetime monitor, in which the electrons from an alpha particle track are collected (see Fig. 2). High purity methane is passed through a bubbler containing TMAE at 28°C, and then through a vessel containing samples of materials in question. The samples have the same surface area as in one drift box/detector assembly, and the nominal operating gas flow rate per drift box of 250 cc/min is used. The gas is then passed to the alpha ionization detector, in which the ionization electrons are drifted through 6 cm of variable strength electric field, and collected on an anode plate. The collected charge varies exponentially with the calculated drift time, with an absorption time that is characteristic of the gas mixture and is typically > 300 μs for pure CH_4 and about 200 μs for TMAE-laden CH_4. Materials inducing electron lifetimes of less than 75% of the baseline value measured with the materials testing chamber empty are deemed unacceptable for construction of parts to be exposed to TMAE in the drift boxes or detectors.

Some of our results, representing many months of tests spanning more than five years of prototyping and construction, are given here, since they may be of interest to the instrument builder. One obvious caveat is that surface cleaning or baking procedures can affect these results.

- All two-component epoxies tested were found to be compatible with TMAE vapors, with the exception of Hardman five-minute epoxy. DP-190,[5] Hysol,[6] and Epon 826[7] + Versamid 140,[8] which are used extensively in constructing our CRID instrumentation, were tested repeatedly and successfully.

5 3M Inc., St. Paul, MN
6 The Dexter Company, Olean, NY
7 Shell Chemical Co., Houston, TX
8 Henkel Inc., Minneapolis, MN

- Homemade fiberglass-epoxy composites were seen to affect electron lifetimes only marginally after vacuum baking at 80°C.
- Commercial fiberglass-epoxy laminates (*e.g.*, fire retardant-free G-10) and etched G10-Copper laminates reduce electron lifetimes by factors of 1.5 to 2, even after repeated vacuum baking at 80°C. Coating all etched or machined surfaces with a thin layer of DP-190 eliminates this effect.
- Gold-plated, tin-plated, and alodined metal surfaces passed the test. However, etched Beryllium-Copper arrays, which we use to define the potentials on the drift box windows and as optical blinds in the electron detectors, reduce electron lifetimes by factors of 2 to 10, probably due to residue from the etching process. Tin-plating or electropolishing the etched components totally eliminated the effect.
- Amongst valve seat and O-ring materials, we discarded Buna-N rubber because it is readily attacked by TMAE in the liquid phase; we found Kalrez-F O-rings to have no effect on electron drift; Viton VO 747-75[9] has no measurable effect when used as an O-ring in the testing vessel, but has a barely measurable effect when about 100 cm^2 of O-ring is exposed to the TMAE vapor.

VIII. Liquid Radiator Materials and Recirculator System Tests

Proper operation of liquid radiators in the CRID requires a heavy liquid highly transparent to ultraviolet light in the wavelength region between 160 and 220 nm. We have developed a method to measure this transparency for the manufacturer-supplied fluorocarbon (C_6F_{14}), for fluorocarbon which has undergone an initial purification process, and for the liquid as it ages within the radiators and is repurified by a recirculation/filtration process.

The measurement technique uses a 1 cm absorption path in a quartz cell; a monochromator under a nitrogen purge is used to select the wavelengths of interest from a deuterium light source. The light beam then passes through a quartz beam splitter that deflects about half of it to a photomultiplier tube, while the remainder passes through the quartz sample cell and impinges on a second photomultiplier. The ratio of the intensity of light transmitted through the cell to that deflected by the beam splitter is made both for the cell filled with fluorocarbon and purged with boiloff nitrogen. These measurements give the fraction of UV light transmitted through the fluorocarbon relative to nitrogen gas—a measurement largely independent of effects of the beam splitter, the light source, and absorption by the cell quartz windows.

The device which recirculates and purifies the fluorocarbon consists of a reservoir held at 40°C connected to a high-capacity condenser at −40°C. Boil-off nitrogen is initially bubbled through the fluorocarbon to deoxygenate it without loss of appreciable amounts of liquid. This process proceeds at a rate of about 10 liters/hour and reduces the oxygen content from 102,000 ppb (by weight) to about 15 ppb, with a loss of less than 1% of the liquid. After this deoxygenation, the liquid is pumped around a loop containing Oxisorb[10] chemical filters and Zitex[11] Teflon particulate filters. After approximately four to five passes around the loop, the UV transparency has improved from about 0.3 to 0.6 in the 160 to190 nm region, and from about 0.96 to 0.98 in the region between 190 and 220 nm, relative to what it was when originally received from the manufacturer.[12] Results are shown on fig. 12.

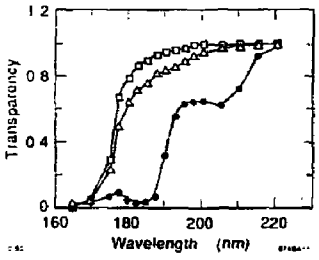

Fig. 12 Transmission of 1 cm of cleaned liquid C_6F_{14} (squares), C_6F_{14} exposed to DP-190 for 107 days (circles), and C_6F_{14} exposed to G-10 for 128 days (triangles).

To understand the aging and recleaning properties of radiators in continuous use, we tested the two major components used in building the liquid radiators, G-10 and DP-190, suspecting possible outgasing, leaching, or reactivity that could affect the UV transparency of the liquid. The materials were immersed in previously-cleaned fluorocarbon and stored in two separate, sealed, electropolished stainless steel containers, maintained at 40°C and constantly stirred. Samples from these containers were tested at ever-lengthening time intervals, permitting contaminants to build up without any recirculation. The G-10 remained in the fluorocarbon for a total of 128 days, whereas the DP-190 was sealed for 107 days. The time-dependent effects of the contaminants on the UV spectrum are also shown in fig. 12, where a mild G-10 effect and a rather drastic DP-190 effect are seen.

9 Parker, Inc., Lexington, KY

10 Messer Griesheim GMBH, D-4000 Düsseldorf 30, FRG

11 Norton Performance Plastics, Wayne, NJ

12 RTZ Chemical, ISC division, Bristol, UK

We then tested the ability of the recirculator to restore the clarity of the liquid. It was recirculated through the filters at 4cc/sec for a time corresponding to 12 filtering passes for the G-10 and 22 passes for the DP-190. In both cases, the transparency spectrum returned to its original cleaned character, within a small systematic error of about 2%. There was some evidence for a loss of transparency of this order. In normal operation, the entire system volume will be filtered every hour; thus, increased opacity of the fluorocarbon in the wavelength regions of interest is not anticipated.

IX. Conclusion

Installation of components of the SLD barrel CRID is proceeding. The fiber optic calibration system for drift boxes has been tested and works as designed. The gating system has been tested and found to be very effective. Drift path distortions are small throughout two production drift boxes. The electron lifetime in the drift boxes is long compared to their length. The materials used in construction of the components have minimal effect on the electron lifetime. The liquid radiator fluorocarbon will remain transparent with recirculation through a filtering loop.

Acknowledgments

The work described here would not have been possible without the assistance of the engineering and technical staffs of the collaborating institutions. Their contributions are gratefully acknowledged.

References

[1] SLD Design Report SLAC 273 UC-34D, May 1984, and revisions; D. Aston *et al.*, *Nucl. Instrum. Methods*, **A283**, 582-589 (1989), SLAC PUB 4795

[2] K. Abe et al., SLAC PUB-5214 (1990).

[3] D. Aston *et al.*, *Nucl. Instrum. Methods*, **A283**, 590 595 (1989), SLAC-PUB-4875 ; see also J. Va'vra *et al.*, *IEEE Trans. Nucl. Sci.* **NS-35**, 487-492 (1988), SLAC-PUB-4432.

[4] E. Spencer *et al.*, *IEEE Trans. Nucl. Sci.* **NS-35**, 231 236 (1988), SLAC-PUB-4404; and P. Antilogus *et al.*, "Cerenkov Ring Imaging Detector Front End Electronics," this conference, SLAC PUB-5120 (1990).

[5] M. Cavalli-Sforza *et al.*, *IEEE Trans. Nucl. Sci.* **NS-37**, 1132-1142 (1990), SLAC-PUB 5123; and K. Abe *et al.*, SLAC-PUB-5199 (1990), submitted to *Nucl. Instrum. Methods* **A**.

[6] D. Aston et al., SLAC-PUB-4785, *IEEE Trans. Nucl Sci.* **NS 36**, 276-282 (1989).

[7] "CRID Nanoammeter Monitoring System," to be published.

[8] D. Fraissard et al., *Nucl. Instr. Meth.* **A252**, 521 (1986).

[9] R. T. Rewick, M. Schumaker, S. Sapiro, T. Weber and M. Cavalli-Sforza, "Tetrakis (Dimethylamino) Ethylene: Identification of Impurities and Compatibility with Common Metal, Polymer, and Ceramic Laboratory Materials," Anal. Chem. **60**, 2095 (1989)